Available online at www.sciencedirect.com
ScienceDirect
Journal of the European Ceramic Society 31 (2011) 1803–1810
www.elsevier.com/locate/jeurceramsoc

Self-assembled microstructured polymeric and ceramic surfaces

Michael Woiton [a,*], Madeleine Heyder [a], Alexandra Laskowsky [b], Edda Stern [a], Michael Scheffler [b], Christoph J. Brabec [a,c]

[a] *Bavarian Center for Applied Energy Research (ZAE Bayern), Am Weichselgarten 7, D-91058 Erlangen, Germany*
[b] *University of Magdeburg, Institute of Materials and Joining Technology, Universitaetsplatz 2, D-39106 Magdeburg, Germany*
[c] *Institute of Materials for Electronics and Energy Technology, University of Erlangen-Nürnberg, Martensstr. 7, D-91058 Erlangen, Germany*

Received 12 August 2010; received in revised form 18 February 2011; accepted 1 March 2011
Available online 2 April 2011

Abstract

Self-assembled microstructures were manufactured by dip coating of substrates with unfilled and filler-loaded preceramic polymer mixtures in the presence of a solvent and a non-solvent. The nature of the polymers was characterized by their solubility parameters. Variation of the polymer/polymer ratio and the volume fraction of the solvent and/or non-solvent led to different surface structures. Studies of the structure formation mechanism indicate that demixing processes of the polymers are responsible for self-assembly in filler-free mixtures. In filler-loaded mixtures the structure formation process, however, is more complex. The micro-structured polymeric coatings obtained from filler loaded systems were converted into polymer derived ceramic coatings under shape retention. High specific surface areas were measured after thermal conversion.

Keywords: Films; Self-assembly; Precursors-organic; Porosity; Surfaces; SiC

1. Introduction

Ceramic coatings are of immense interest for a great variety of applications. They might be used in protection against corrosion and abrasion, as thermal barrier coatings, as functional coatings in energy conversion devices such as anti-reflexion coatings in solar cells or as catalytically active material or support.[1] Among the coating processes thermal spraying,[2] CVD,[3] PVD,[4] and sol–gel processing[5,6] are the most common to be applied on an industrial scale. In the past few years preceramic polymers or particle-filled preceramic polymers gained interest as starting materials for ceramic coatings due to their unique combination of low temperature processing capability, versatile shaping, as well as microstructure and property tailoring capabilities. A topical overview is given in Ref. [7].

Processing of preceramic polymers into ceramic products involves shaping of a low viscosity polymeric precursor followed by curing and pyrolysis at temperatures above 800 °C. Due to the pronounced density differences between the polymer (1–1.2 g cm^{-3}) and the ceramic phases (2–3 g cm^{-3}) shrinkage of up to 70 vol.% may occur which gives rise to extended porosity formation or even cracking in the pyrolysed ceramic residue material. Oxide, non-oxide or metallic/intermetallic filler powders may be used for shrinkage compensation.[8]

Most of the preceramic polymer coatings are based on polycarbosilanes,[9,10] polysilazanes,[11–13] or polysiloxanes,[14–16] and they are applied by spin or dip coating.

A novel processing method for ceramic coatings based on preceramic polymers takes advantage of dewetting and demixing processes of two different preceramic polymers. This was shown for the first time in Ref. [17]. Surface structures in micrometre scale were prepared on different substrates by a coating process using particle-filled slurries based on a blend of two preceramic polymers. Parameters such as solvent fraction, substrate material, filler particle size, and layer thickness were varied. Demixing reactions of solvent and polymers led to surface structures with pores of 1–60 μm in diameter. As the key to describing the structure formation the solubility parameters of the polysiloxanes used as preceramic polymers were measured.

* Corresponding author. Tel.: +49 9131 691 177; fax: +49 9131 691 181.
E-mail address: woiton@zae.uni-erlangen.de (M. Woiton).

0955-2219/$ – see front matter © 2011 Elsevier Ltd. All rights reserved.
doi:10.1016/j.jeurceramsoc.2011.03.001

However, the basic mechanisms responsible for the formation of the structure were not revealed.The solubility parameters describe the miscibility or immiscibility of two components. According to the principle "like dissolves like" *Hildebrand* introduced the *Hildebrand*-solubility parameter basing on the cohesive energy density. For a good interaction of the solvent and the polymer the *Hildebrand*-solubility parameters should have approximately the same value. But the *Hildebrand*-solubility parameter is only valid for nonpolar solvents. Therefore *Hansen* divided the solubility parameter into the dispersion component (δ_d), polar component (δ_p), and hydrogen-bonding component (δ_h), the so-called *Hansen*-solubility parameter (HSP). If for two substances all three values are similar they may be assumed to be miscible.[18–21]

In this work correlation between phase diagrams, solubility parameters, and the composition of the solution with the self-assembled structure of the coatings was established for the first time. Differences in surface structure formation in unfilled and filled systems were found. Pyrolysis of selected green samples actually resulted in the formation of microstructured ceramic coatings that preserved the physical coating structure of the polymeric surface coating.

2. Experimental

Coatings were produced from a filled slurry with well-known properties from previous investigations to minimize unexpected effects[17,22–24]. The silicon components were 9.2 vol.% polymethylphenylvinylsiloxane (PMPS, Silres H62C, $[(C_6H_5)_{0.44}(CH_3)_{0.24}(C_2H_3)_{0.16}H_{0.16}SiO_{1.5}]_n$) and 9.2 vol.% polymethylsiloxane (PMS, Silres MK, $[CH_3SiO_{1.5}]_n$, both Wacker Chemie GmbH, Munich, Germany). 8.1 vol.% methyltriethoxysilane (MTES, $[(C_2H_5O)_3SiCH_3]$, Wacker-Chemie GmbH, Munich, Germany) and 53.8 vol.% methanol (MeOH, ROTIPURAN® ≥ 99.9%, $[CH_3OH]$ Carl Roth GmbH + Co. KG, Karlsruhe, Germany) were used as solvents. The crosslinking catalysts were 1.1 vol.% oleic acid ($C_{18}H_{34}O_2$) and 0.6 vol.% aluminium acetylacetonate ($C_{15}H_{21}AlO_6$, both compounds from Merck KGaA, Darmstadt, Germany), while the filler material was 18.1 vol.% silicon carbide (SiC, SM07, d_{50} 1.3–1.7 μm, ESK-SiC GmbH, Frechen, Germany).

PMPS was dissolved in MTES by stirring with a magnetic stirrer. After 10 min PMS was added and stirring was continued for another 2 h, i.e. until it was completely dissolved. MeOH was added and the solution was stirred for another 30 min. After that the filler material SiC was added and stirring was continued for another 15 min. The crosslinking catalysts were added in the final step. All components were homogenized by vigorous stirring for 18 h with a magnetic stirrer.

Before starting the dip coating process the slurry was homogenized by sonication for 10 min. Al_2O_3 tapes (Keral 96, KERAFOL Keramische Folien GmbH, Eschenbach, Germany) were used as substrates. Additionally, the slurry was stirred with the magnetic stirrer for 2 min before each individual dip coating process. The dip coating speed was 23.1 mm s^{-1} with 1 s exposure time in the slurry before withdrawal.

Table 1
Basic compositions.

Composition	PMS [vol.%]	PMPS [vol.%]	MTES [vol.%]
COMP01	33.3	33.3	33.3
COMP02	60.0	20.0	20.0
COMP03	20.0	60.0	20.0
COMP04	20.0	20.0	60.0

The samples were dried for 24 h at 30 °C and cross-linked for 24 h at 110 °C in a drying furnace (TR 120, Nabertherm GmbH, Lilienthal, Germany).

Four basic compositions from PMS, PMPS and MTES were prepared to analyse the correlation between composition and morphology. The base compositions are given in Table 1. A dilution series in MeOH was prepared from composition COMP1, varying the concentration from 10 to 90 vol.% in 10% steps. The four basic compositions as well as the dilution series were prepared as noted above, with the only difference that no filler was added.

UV–Vis spectroscopy (wavelength: 550 nm, Cary 500 Scan, Varian Inc., Palo Alto, USA) was used to analyse the phase separation of the MeOH-containing samples. For this purpose slurries of the dilution series were tested on their turbidity, using the basic composition COMP1 without MeOH as baseline.

To get information about the miscibility in the quaternary system MTES–PMPS–PMS–MeOH, the concentrations of the four components were varied in 16.67 vol.% steps. The mixtures were prepared by stirring for 15 min followed by sonication for 10 min transparent mixtures were taken as miscible while turbid mixtures were taken as immiscible.

Hansen-solubility parameters (HSPs) of the polysiloxanes were determined by dissolution experiments using solvents with different solubility parameters.[21] For these experiments a polymer concentration of 50 vol.% was chosen. Only solvents resulting in a completely clear mixture were considered as "solvent". The *Hansen*-solubility parameters and the spheres were calculated with MATLAB using the *Gharagheizi* software package.[25] For the calculation of the polymers solubility parameters all HSPs of the solvents where plotted in a three-dimensional chart by using their three parameters as axes. After this a sphere was constructed including all solvents excluding all non-solvents. The HSPs of the polymers are given by the centres of the spheres and the volume of interaction is given by the volume of the sphere.

Thin film coatings were characterized by optical microscopy (AxioImager.M1m, Carl Zeiss MicroImaging GmbH, Jena, Germany). Incident light and dark filed images were made with a 25-, 100-, 200-, 500-, and 1000-fold magnification. Depth resolution was improved by combining a stack of images by the software AxioVisio (V 4.8.1, Carl Zeiss MicroImaging GmbH, Jena, Germany) into one image. High resolution Scanning Electron Microscopy (SEM) images were taken with a JSM 6400 (Jeol Ltd., Tokio, Japan). The composition of films was analysed by energy-dispersive X-ray analysis (EDX). All images including the optical microscope images were taken after cross-

Table 2
Solvents and their solubility parameters,[20] classification in solvents (1) and non-solvents (0) for PMS and PMPS.

Solvent	Dispersion δ_d [MPa$^{1/2}$]	Polarity δ_p [MPa$^{1/2}$]	Hydrogen bonding δ_h [MPa$^{1/2}$]	PMS	PMPS
1,3-Propanediol	16.8	13.5	23.2	0	0
1,4-Dichlorobutane	18.3	7.7	2.8	0	1
1-Methyl-2-pyrrolidinone	18	12.3	7.2	0	1
2-Butanol	15.8	5.7	14.5	0	0
2-Propanol	15.8	6.1	16.4	0	0
4-Hydroxy-4-methylpentan-2-one	15.8	8.2	10.8	0	1
Acetic acid	14.5	8	13.5	0	0
Acetone	15.5	10.4	7	0	1
Benzoyl chloride	20.7	8.2	4.5	0	1
Cyclopentane	16.4	0	1.8	1	0
Diethyl carbonate	15.1	6.3	3.5	0	0
Diethylene glycol	16.2	14.7	20.5	0	0
Diethylene glycol butyl ether acetate	16	4.1	8.2	1	1
Ethanol	15.8	8.8	19.4	0	0
Ethanolamine	17	15.5	21.2	0	0
Ethylene cyanohydrin	17.2	18.8	17.6	0	0
Furfuryl alcohol	17.4	7.6	15.1	0	0
Isophorone	16.6	8.2	7.4	1	1
Mesityl oxide	16.4	6.1	6.1	1	1
Mesitylene	18	0	0.6	1	0
Methanol	15.1	12.3	22.3	0	0
Methyl ethyl ketone	16	9	5.1	0	1
n-Hexane	14.9	0	0	0	0
Nitroethane	16	15.5	4.5	0	1
Oleic acid	14.3	3.1	14.3	0	0
Water	15.5	16	42.3	0	0

linking, except the right image in Fig. 8 which was taken after pyrolysis.

Selected samples were pyrolysed in nitrogen atmosphere with a heating rate of 1 K min^{-1} at 1100 °C and a dwell time of 2 h (LOSIC, HTM Reetz GmbH, Berlin, Germany). After pyrolysis these samples were characterized by SEM and by nitrogen adsorption with an ASAP 2000 (Micromeritics, Inc.).

Table 3
Solubility parameters of PMS and PMPS.

Polymer	Dispersion δ_d [MPa$^{1/2}$]	Polarity δ_p [MPa$^{1/2}$]	Hydrogen bonding δ_h [MPa$^{1/2}$]	Radius *RA* [MPa$^{1/2}$]
PMS	17.7	1.4	7.6	7.6
PMPS	20.6	11.6	5.1	12.2

3. Results and discussion

3.1. Characterization of starting materials

Table 2 shows the solvents used for determining the *Hansen*-solubility parameters (HSPs) of the polymers. They are classified in solvents (marked with "1") and non-solvents (marked with "0") with respect to the polymers. Only three solvents, diethylene glycol butyl ether acetate, isophorone, and mesityl oxide, have been identified to be useful for both polymers, polymethylsiloxane (PMS) and polymethylphenylvinylsiloxane (PMPS). Also methyltriethoxysilane (MTES) could be identified as a solvent for both polymers, but it is not in the table because of the lack in data for its HSP.

Fig. 1 shows the volume of interaction of the particular polymer. All pluses inside the sphere indicate that the polymer is soluble in the solvent investigated. Crosses outside the sphere indicate no solubility. A considerably larger volume of interaction was identified for PMPS than for PMS which is also given by the larger radius of interaction of 12.2 MPa$^{1/2}$ for PMPS and 7.6 MPa$^{1/2}$ for PMS.

The centres of the spheres give the solubility parameters of the polymer itself which are also displayed in Table 3. The centre of the PMS sphere is located close to the boundary of the sphere of PMPS and vice versa which is also indicated by the difference in the solubility parameters of the polymers especially in the polarity component. The solubility parameters, particularly the polarity component, suggest an incompatibility of the two polymers PMS and PMPS which is an indication for a polymer/polymer demixing process.

By using the solubility parameters methanol (MeOH) could be identified as a non-solvent for both polymers PMS and PMPS.

The phase diagrams shown in Fig. 2 visualize the miscibility in the quaternary system (tetrahedron) MTES–PMPS–PMS–MeOH. Each of the four phase diagrams shows a different level of the MeOH concentration from 0 to 50 vol.% in 16.67 vol.% steps of this tetrahedron. The ternary system PMPS–PMS–MeOH presented by the bottom axes of the phase diagrams, shows no miscibility at all. This is also true for the included binary systems of PMPS–PMS (bottom axis in the 0% MeOH chart), PMS–MeOH (lower right corner of the charts), and PMPS–MeOH (lower left corner

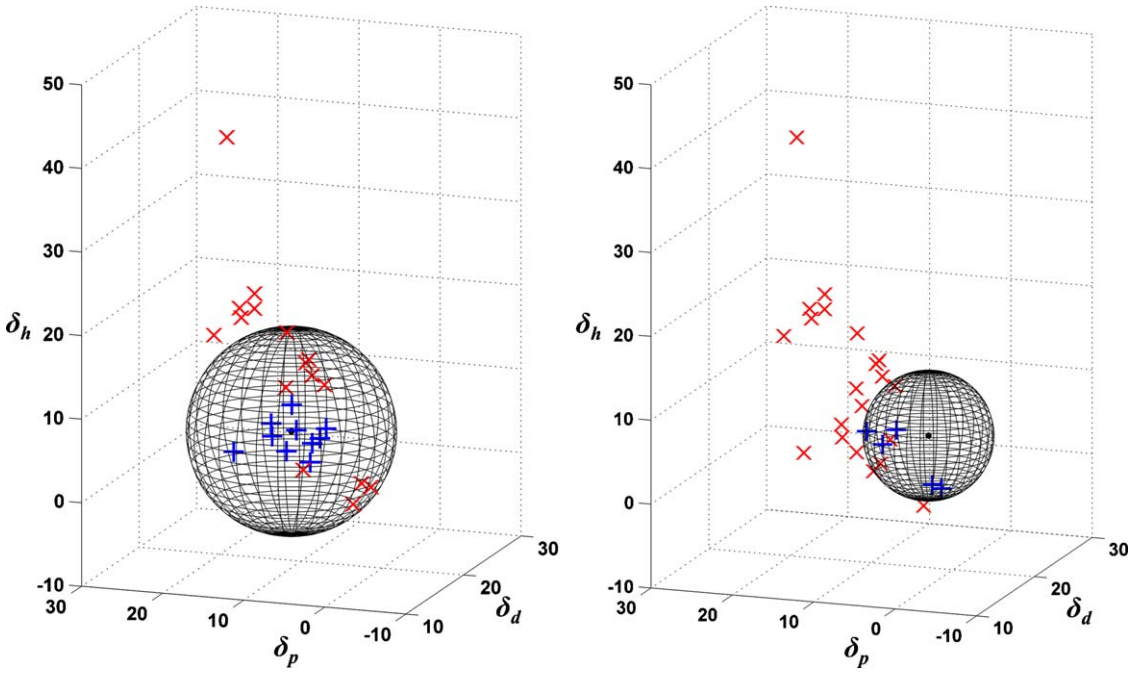

Fig. 1. Solubility spheres of PMS (left) and PMPS (right). All solvents inside the spheres (+) are dissolving the polymers while all solvents outside the spheres (×) do not dissolve the polymers. The centres of the spheres give the solubility parameters of the polymers.

of the charts) which are not miscible too. Only compositions containing MTES show miscibility. With an increase of the PMS concentration accompanied by a decrease of the MTES concentration the miscibility decreases.

Therefore MTES in this system is needed as solvent, because only mixtures with MTES are miscible. In contrast, MeOH can be identified as a "non-solvent" for the system, because there is no solution composition with MeOH as the only sol-

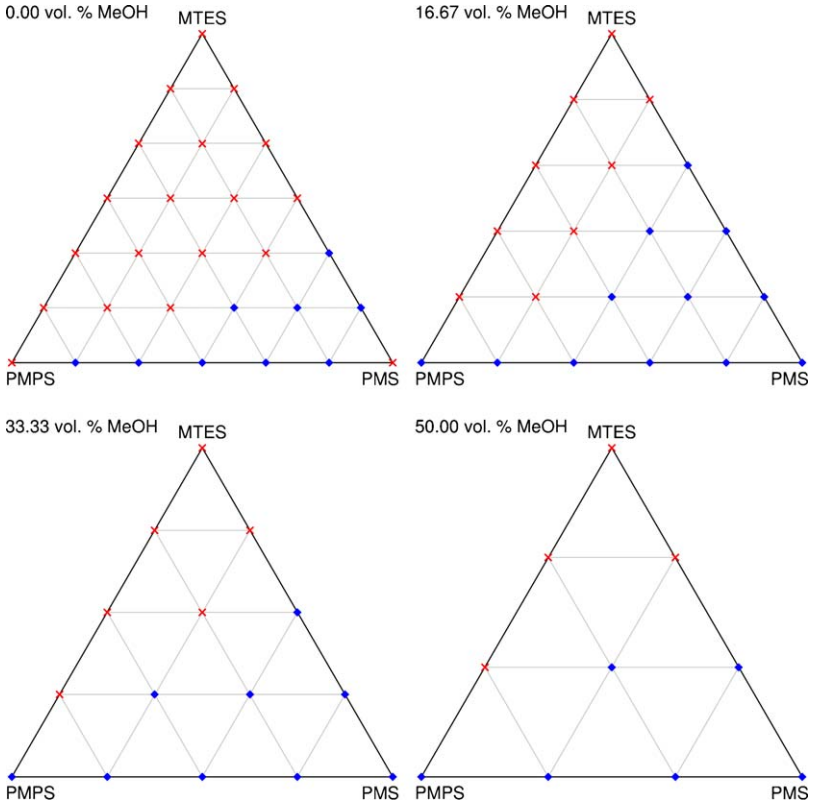

Fig. 2. Phase diagram for different levels of MeOH concentrations of the quaternary system (tetrahedron) MTES–PMPS–PMS–MeOH 0 vol.% (upper left), 16.67 vol.% (upper right), 33.3 vol.% (lower left), and 50 vol.% (lower right). (♦) Immiscible samples; (×) miscible samples.

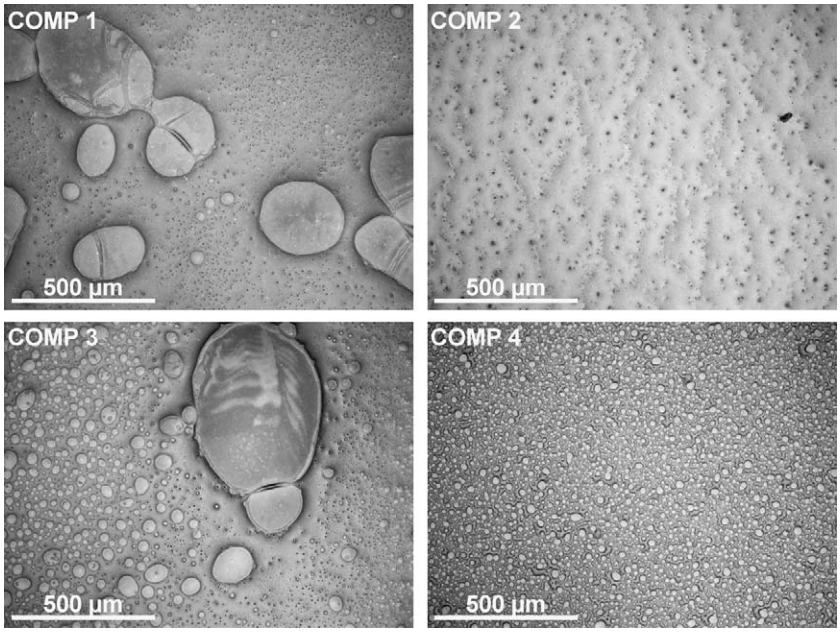

Fig. 3. Microscope images of compositions from PMS, PMPS and MTES (Table 1). The ratio of PMS to PMPS is COMP1 33:33, COMP2 60:20, COMP3 20:60, and COMP4 20:20. The ratio is given in vol.%. The balance is the amount of MTES.

vent. Moreover, mixtures with high MeOH concentrations show no miscibility. This is consistent with the solubility parameter where MTES could be identified as a solvent and MeOH as a non-solvent. Also the immiscibility of the two polymers PMS and PMPS could be shown by both the phase diagrams and the HSPs.

3.2. Filler-free layers

Light microscope images, cf. Fig. 3, show filler free layers of COMP1–COMP4, prepared on alumina tapes. Different compositions caused different layer structures. The layer of COMP1 shows big islands surrounded by a matrix with a number of small islands. The image of COMP2 shows a structure with small islands embedded in a matrix with topography similar to mountain ridges. COMP3 shows a similar structure like COMP1, big islands surrounded by a matrix with numerous small islands. In COMP3 the smaller islands are bigger than in COMP1 and the total area covered with islands in COMP3 is larger than the area in COMP1. The image of COMP4 provides a uniform structure with many islands of the same size embedded in the matrix.

When comparing the size and number of the islands, it is evident that samples with a higher amount of PMPS have more and bigger islands. COMP3 with the highest amount of PMPS shows more and bigger islands than COMP2 with the lowest amount of PMPS. This was also found for the comparison of COMP3 with COMP1 and COMP4. Therefore it can be assumed that PMPS builds the islands and PMS is the main component of the matrix. This was also proven by SEM and EDX with a sample containing a COMP4 coating.

The SEM image in Fig. 4 shows the same structure as the optical microscope image in Fig. 3 (below, right). The chart (Fig. 4 below) of the EDX analysis along the line L1 (top image) shows different compositions for the bright matrix and the dark islands. The islands have a higher amount of carbon and lower amounts of silicon and oxygen, cf. Fig. 4, bottom. In contrast, the matrix has higher amounts of silicon and oxygen and a lower amount of carbon. The chart also shows that the amount of aluminium is always close to zero which means that the alumina substrate is completely covered by the polymer layer.

PMS has a molecular composition described with the formula $[CH_3SiO_{1.5}]_n$. PMPS possesses a composition described by $[C_{3.21}H_{3.56}SiO_{1.5}]_n$. PMPS contains more carbon, less silicon, and less oxygen than PMS. Therefore we suggest PMS to be the dominant compound in the matrix, while PMPS is the

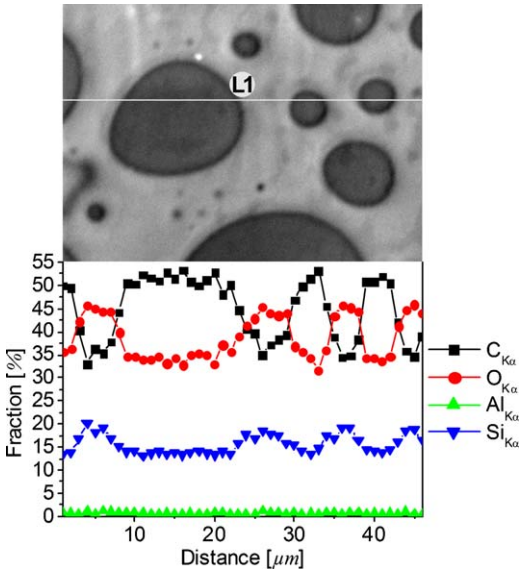

Fig. 4. SEM image of a layer from COMP4 on an alumina tape (above). The line L1 shows the path of the EDX analysis in 1 µm steps in the chart below.

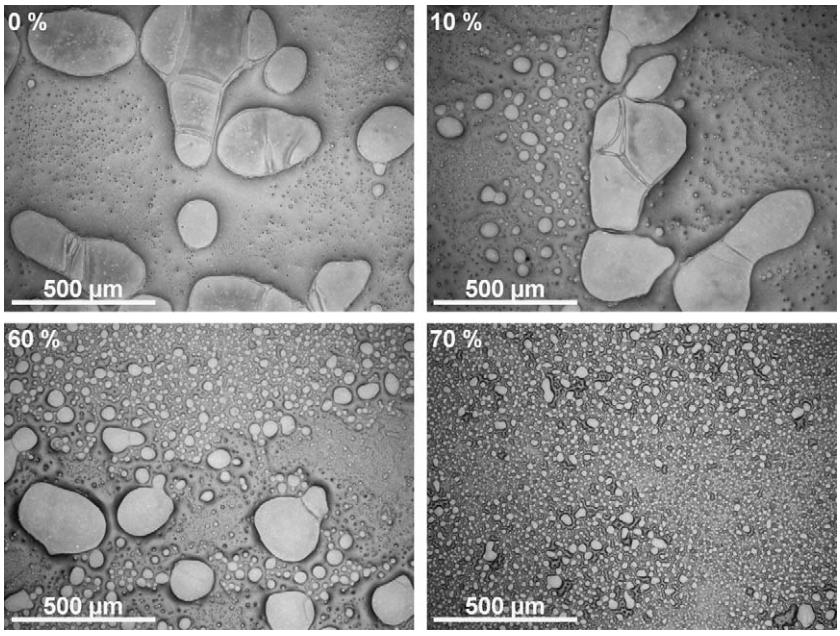

Fig. 5. Microscope images of COMP1 on alumina tapes with different volume fractions of MeOH.

dominant component of the islands. These findings are in good agreement with the microscope images, Fig. 3, for the different compositions.

Since the composition of the matrix and the islands are different this indicates that a polymer/polymer demixing process is involved in the structure formation process. This is in good accordance with the HSP and the phase diagrams, which also indicate a polymer/polymer incompatibility. In the phase diagrams the origins of COMP1, COMP3, and COMP4 are in the area where miscible compositions are located. But during the drying process the solvent MTES evaporates and the composition moves into the immiscible area.

Light microscope images in Fig. 5 show how the addition of MeOH can modify the structure of filler free coating. The MeOH fraction in COMP1 was varied from 0 to 90 vol.%. Little or no influence on the structure formation was observed for MeOH concentrations between 10 and 60 vol.%. Upon increasing of the MeOH concentration, smaller islands of equal size are formed with some homogeneity all over the sample, similar to that of COMP4.

Fig. 6 shows the Vis transmission of the solutions of COMP1 at 550 nm with varying MeOH volume fraction. From 0 to 60 vol.% MeOH the transmission decreases slightly from 100% to 96.4%. Mixtures with a MeOH fraction of more than 60 vol.%, however, show significantly reduced transmission, and mixtures with a fraction of more than 80 vol.% could not anymore be characterized because of strong scattering due to spontaneous phase separation. These characteristics are in accordance with those found for the layers formed, which show the same structure from mixtures with 10–60 vol.% MeOH and a different structure with fractions higher than 60 vol.% MeOH.

In conclusion, we find that the structure formation in filler free systems is dominated by a polymer/polymer demixing process, which could be shown by the HSP, the phase diagrams and the

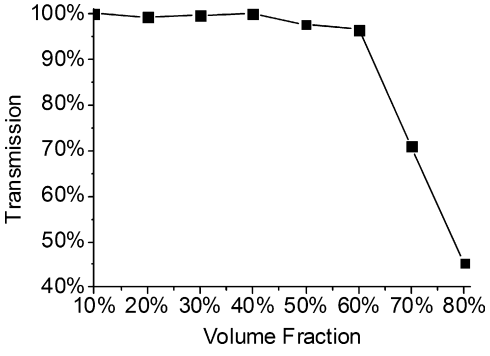

Fig. 6. Chart of UV–Vis transmission at 550 nm of COMP1 with different volume fractions of MeOH.

EDX analysis. MTES is necessary as solvent for both polymers. MeOH, on the other hand, was identified as a non-solvent for both polymers and actually could be proven not to be relevant for the structure formation due to phase separation, because the structure formation with and without MeOH is almost the same. Only at very high concentrations MeOH cause a less coarse phase separation between the two polymers.

3.3. Filler-loaded layers

In another set of experiments the influence of particulate fillers on the structure formation was investigated. The SEM images on SiC filled coatings as shown in Fig. 7 show the typical structures which are known for particle-filled systems,[17] i.e. they are dominated by almost ringlike pores which are separated by ligaments. The SiC particles have clearly been identified to be within and on the ligaments as well as on the bottom of the pores.

Since SiC particles are visible all over the SEM image, especially also at the bottom of the coating, it is obvious that these

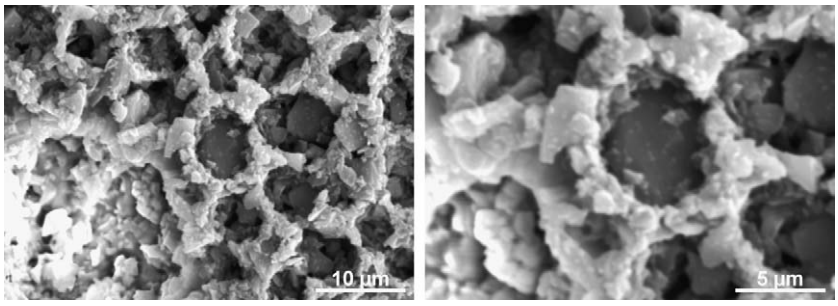

Fig. 7. SEM images of SiC filled layers on alumina tapes. The round pores surrounded by ligaments and the SiC particles are visible.

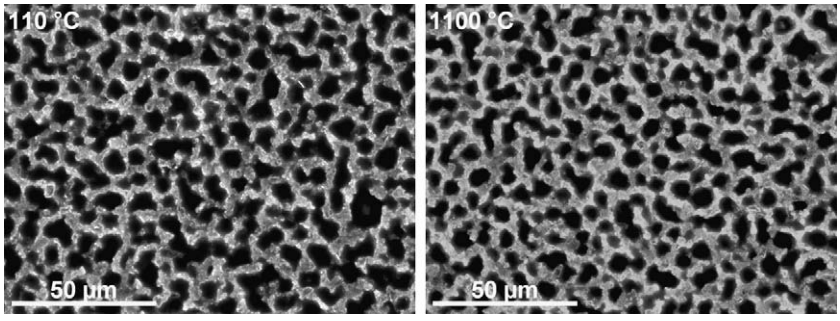

Fig. 8. Microscope images of a sample after drying at 110 °C (left) and after pyrolysis at 1100 °C in nitrogen atmosphere (right).

features are real pores. If the pores would be filled, for example with polymer, the SiC particles on the bottom of the pores would not be visible in a SEM image. From this we conclude that the addition of fillers (i.e. SiC) causes a significant change in the structure of these coating composites. While the structure of unfilled systems is dominated by the phase separation of the two polymers, the filled systems are dominated by hollow pores, also addressed as holes. The hole formation might be initiated by a different process, which is related to the presence of the filler.

For a deeper understanding of the hole formation mechanism compositions were prepared with fillers and different MeOH concentrations. No significant hole formation was observed for MeOH volume fractions below 53.8 vol.%. Increasing the MeOH volume fraction to 53.8 vol.% and higher finally resulted in the formation of the hole structure.

The MeOH fraction of 53.8 vol.% corresponds to 65.7 vol.% after subtraction of filler material. This is close to the fraction of 60 vol.% in filler free systems at which the structure begins to change and the optical transmission (cf. Fig. 6) starts to decrease considerably.

Thus, MeOH plays an important role for the structure formation in filled systems and influences the structure formation in filler free systems. In filled systems it is necessary for the structure formation, without MeOH no hole structure was formed. In filler free systems MeOH is not mandatory for the structure formation, but on the other hand it has an influence on it at higher concentrations.

Finally the shape retention during thermal conversion was proven for coatings on alumina. As an example, Fig. 8 shows a microscope image of a sample dried at 110 °C (left) and pyrolysed at 1100 °C (right). Good shape retention was found.

The specific surface area shows a dependence on the coating thickness of these samples which is varied by the withdrawal speed. It was between 60 $m^2\,g^{-1}$ and 165 $m^2\,g^{-1}$.

Due to their structural features in the micrometre range after thermal conversion at high temperatures these coatings are suggested for potential use as catalyst support, as heat storage active-component support or as substrate material for thin film silicon photovoltaic with improved light trapping properties.

4. Conclusion

We have investigated the basic structure formation mechanisms in unfilled and filled polysiloxane-type preceramic polymer coatings. In unfilled systems it has been shown that structure formation is initiated and dominated by phase separation processes of the starting polymers PMS and PMPS. The phase separation of these two polymers is in good agreement with the phase diagrams and their solubility parameters, which were calculated from their *Hansen*-spheres.

The structure formation in filled systems, however, is more complex and might be summarized as follows:

- the structure of filled PMPS, PMS or blends thereof was found to be dominated by holes,
- the polymer/polymer demixing process, might not be relevant for the formation of the holes, and
- a mixture of SiC particles as fillers in combination with MeOH as non-solvent was identified as the driving force towards hole formation.

The non-solvent MeOH was found to significantly influence structure formation in both, filled and unfilled, systems. High

concentrations of MeOH affect the structure in unfilled systems and in filled systems MeOH is crucial for the hole formation.

Acknowledgments

The authors gratefully thank the German Research Foundation (STE 1885/1-1 and SCHE 628/8-1) for financial support. We also thank A. Lloyd, S. Schön, T. Zehnder (ZAE Bayern, Erlangen) for providing experimental data and helpful discussions. A special thank is given to F. Scheffler (Univ. of Magdeburg) for nitrogen adsorption measurements, and thanks to E. Völkel (Univ. of Erlangen-Nürnberg) for SEM investigations. Thanks also to J. Schneibel (Univ. of Magdeburg, now with the ORNL, TN, USA) for proof reading the manuscript.

References

1. Majumdar A, Sunirmal J. Glass and glass–ceramic coatings, versatile materials for industrial and engineering applications. *Bull Mater Sci* 2001;**24**:69–77.
2. Limarga AM, Widjaja S, Yip TH. Mechanical properties and oxidation resistance of plasma-sprayed multilayered Al_2O_3/ZrO_2 thermal barrier coatings. *Surf Coat Technol* 2005;**197**:93–102.
3. Probst D, Hoche H, Zhou Y, Hauser R, Stelzner T, Scheerer H, et al. Development of PE-CVD Si/C/N:H films for tribological and corrosive complex-load conditions. *Surf Coat Technol* 2005;**200**:355–9.
4. Allebrandt D, Hoche H, Scheerer H, Broszeit E, Berger C. Oxidation resistance of SiAlCN: H-coatings. *Surf Coat Technol* 2007;**201**:5172–5.
5. Izumi K, Minami N, Uchida Y. Sol–gel-derived coatings on steel sheets. *Key Eng Mater* 1998;**150**:77–88.
6. de Sanctis O, Gómez L, Pellegri N, Parodi C, Marajofsky A, Durán A. Protective glass coatings on metallic substrates. *J Non-Cryst Solids* 1990;**121**:338–43.
7. Scheffler F, Torrey JD. Coatings. In: Colombo P, Soraru GD, Riedel R, Kleebe H, editors. *Polymer derived ceramics: from nano-structure to applications.*. Lancaster, PA: DEStech Publications; 2009. p. 358–68.
8. Greil P. Polymer derived engineering ceramics. *Adv Eng Mater* 2000;**2**:339–48.
9. Colombo P, Paulson TE, Pantano CG. Synthesis of silicon carbide thin films with polycarbosilane (PCS). *J Am Ceram Soc* 1997;**80**:2333–40.
10. Colombo P, Paulson TE, Pantano CG. Atmosphere effects in the processing of silicon carbide and silicon oxycarbide thin films and coatings. *J Sol–Gel Sci Technol* 1994;**2**:601–4.
11. Kroke E, Li Y, Konetschny C, Lecomte E, Fasel C, Riedel R. Silazane derived ceramics and related materials. *Mater Sci Eng R* 2000;**26**:97–199.
12. Günthner M, Kraus T, Krenkel W, Motz G, Dierdorf A, Decker D. Particle-filled PHPS silazane-based coatings on steel. *Int J Appl Ceram Technol* 2009;**6**:373–80.
13. Günthner M, Kraus T, Dierdorf A, Decker D, Krenkel W, Motz G. Advanced coatings on the basis of Si(C)N precursors for protection of steel against oxidation. *J Eur Ceram Soc* 2009;**29**:2061–8.
14. Torrey JD, Bordia R, Henager C, Blum Y, Shin Y, Samuels W. Composite polymer derived ceramic system for oxidizing environments. *J Mater Sci* 2006;**41**:4617–22.
15. Torrey JD, Bordia RK. Processing of polymer-derived ceramic composite coatings on steel. *J Am Ceram Soc* 2008;**91**:41–5.
16. Torrey JD, Bordia RK. Mechanical properties of polymer-derived ceramic composite coatings on steel. *J Eur Ceram Soc* 2008;**28**:253–7.
17. Stern E, Heyder M, Scheffler F. Micropatterned ceramic surfaces by coating with filled preceramic polymers. *J Am Ceram Soc* 2009;**92**:2438–42.
18. Burke J. Solubility parameters: theory and application. In: Jensen C, editor. *AIC book and paper group annual*. Washington: AIC Book and Paper Group; 1984. p. 13–58.
19. Zeng W, Du Y, Xue Y, Frisch HL. Solubility parameters. In: Mark JE, editor. *Physical properties of polymers handbook*. New York, NY: Springer; 2007. p. 289–303.
20. Hansen CM. *Hansen solubility parameters: a user's handbook*. 2nd ed. Boca Raton: CRC Press; 2007.
21. Hansen CM. The universality of the solubility parameter. *Ind Eng Chem Prod Res Dev* 1969;**8**:2–11.
22. Cromme P, Scheffler M, Greil P. Ceramic tapes from preceramic polymers. *Adv Eng Mater* 2002;**4**:873–7.
23. Melcher R, Cromme P, Scheffler M, Greil P. Centrifugal casting of thin-walled ceramic tubes from preceramic polymers. *J Am Ceram Soc* 2003;**86**:1211–3.
24. Scheffler F, Scheffler M. Polymer derived ceramic tapes as substrate and support for zeolites. *Adv Appl Ceram* 2009;**108**:468–75.
25. Gharagheizi F. New procedure to calculate the Hansen solubility parameters of polymers. *J Appl Polym Sci* 2007;**103**:31–6.